The Advection–Diffusion Problem for Stratospheric Flow. Part II: Probability Distribution Function of Tracer Gradients

YONGYUN HU AND RAYMOND T. PIERREHUMBERT

Department of the Geophysical Sciences, University of Chicago, Chicago, Illinois

(Manuscript received 15 May 2001, in final form 25 March 2002)

ABSTRACT

This paper is a continuation of the study of the advection–diffusion problem for stratospheric flow, and deals with the probability distribution function (PDF) of gradients of a freely decaying passive tracer. Theoretical arguments are reviewed and extended showing that mixing of a weakly diffused tracer by random large-scale flows produces a tracer gradient field whose probability distribution function has ''stretched exponential'' tails $P(|\nabla\theta|) \propto \exp(-b|\nabla\theta|^{\gamma})$ with $\gamma < 1$. This contrasts with the lognormal distribution expected for advective mixing in the absence of diffusion. The non-Gaussian distribution of tracer gradients can be derived in terms of the statistics of strain rates of the random driving flow. It is shown that the tails of the gradient PDF provide information about the dissipation scale, the scale selectivity of the dissipation law, and the fluctuations of short-term strain. The gradient PDF is shown to contain information about tracer variability that is not present at all in the power spectrum of the tracer field.

To show that the predictions remain valid for the gradient statistics of passive tracers driven by the well-organized lower-stratospheric flow with mixing barriers, a series of advection–diffusion simulations of a decaying passive tracer are presented. The mixing is driven by ECMWF winds on the 420-K isentropic surface using the high-resolution finite-volume model employed in Part I of this paper. It is found that the probability distribution function of the simulated tracer gradients is indeed stretched exponential, with the stretching parameter $\gamma \approx 0.55$. The largest gradients are not found in the regions of highest Lyapunov exponents, but rather in the surf-zone regions adjacent to the reservoirs of high tracer fluctuation amplitude.

1. Introduction

In Hu and Pierrehumbert (2001, hereafter Part I), we studied the probability distribution function (PDF) of a decaying passive tracer driven by the stratospheric flow. It was found that small-scale, large-amplitude tracer fluctuations are characterized by non-Gaussian PDF tails (nearly exponential). An extensive study of observed PDFs of stratospheric tracers, touching on many of the same themes we have examined theoretically, can be found in Sparling (2000). In the present paper we turn our attention to the PDFs of tracer gradients in the lower stratosphere. Characterization of tracer gradients is important because the gradient distribution can provide information about the aggregate effects of tracer variance dissipation, which occurs on scales that are difficult to observe directly. Further, the dissipation or diffusive scale is the scale at which chemical reactants are actually brought into contact, so that characterization of tracer behavior at this scale can have a bearing on the rate of progress of chemical reactions in an inhomogeneous environment.

There have been a number of attempts to estimate an effective horizontal diffusivity for the stratosphere by using observed properties of tracer filaments. The general idea behind these efforts is that, if one has an estimate of the strain rate due to stratospheric winds, then the thinnest observed filaments allow one to estimate the diffusivity by balancing thinning by strain against broadening by diffusion. The estimate by Waugh et al. (1997) was carried out by balancing strain against horizontal diffusion, but Haynes and Anglade (1997) showed that the dissipation is primarily accomplished by vertical diffusion acting on enhanced vertical gradients; the latter employed quantitative statistical models of the enhancement of vertical gradients in an attempt to estimate vertical diffusivity. Balluch and Haynes (1997) carried the program further, examining case studies of filament evolution in comparison with simulations carried out with various estimates of diffusivity. They pointed out that the maximum gradients at the edge of filaments may provide a better basis for estimating dissipation than the overall width of the filament itself. They also suggested that PDFs of tracer gradients might provide a good basis for such an anal-

Corresponding author address: Dr. Raymond T. Pierrehumbert, Dept. of the Geophysical Sciences, University of Chicago, 5734 S. Ellis Avenue, Chicago, IL 60637.
E-mail: rtp1@midway.uchicago.edu

ysis. In the present work, we develop some of the theoretical underpinnings needed to interpret the PDFs of tracer gradients. In effect, we consider the statistics of tracer gradients that would result from an ensemble of strain–diffusion processes of the sort examined in the case studies in Balluch and Haynes (1997).

Characterizing tracer diffusive dissipation has been one of the main concerns since the very beginning of turbulence research. Gurvich and Yaglom (1967) first suggested that the PDF of local diffusive dissipation rate of a tracer should be lognormal. However, Kraichnan (1974) pointed out that the lognormal distribution of gradients is valid only for the case of nondiffusive tracers in homogeneous turbulent flows, and that diffusive dissipation should cut off the tail of the lognormal distribution. The study of tracer gradient PDFs was reinvigorated in the late 1980s, when intriguing Rayleigh–Benard thermal convection experiments were carried out at the University of Chicago (Castaing et al. 1989). The experimental results stimulated considerable theoretical efforts, and a great deal of theoretical progress has been made on the PDF of tracers and their gradients in turbulence research (Sinai and Yakhot 1989; Yakhot et al. 1990; Shraiman and Siggia 1994; Chertkov et al. 1998; Balkovsky and Falkovich 1998, Balkovsky and Fouxon 1999). The phenomenon of non-Gaussian tracer and gradient PDFs is quite robust, and is encountered for developed 3D turbulence as well as for smoother flows. A review emphasizing the former case can be found in Warhaft (2000). The theory of the PDFs is best developed for the case of advection–diffusion by spatially smooth flow, and this is the case that shall principally concern us in stratospheric applications. For this case, Balkovsky and Fouxon (1999) have shown that the gradients of a stochastically forced tracer have stretched exponential tails, defined by $P(|\nabla\theta|) \propto \exp(-b|\nabla\theta|^{\gamma})$ with $\gamma < 1$.

The freely decaying case is at present unsettled. Balkovsky and Fouxon (1999) do not explicitly discuss the form of the tracer or gradient PDF for the decaying case, but they do present results for the evolution of the moments of the fields [see section 3a of Balkovsky and Fouxon (1999)]. These results imply that the shape of the PDFs evolves with time toward progressively slower decaying, or ''fatter,'' tails. These would qualitatively resemble stretched exponentials with γ evolving toward zero as time goes on. The evolution of the tracer PDF for stratospheric mixing in Part I was consistent with these predictions, at least over the 60-day timescale. However, the long-term simulations (albeit with more idealized flows) described in Pierrehumbert (2000) are inconsistent with Balkovsky and Fouxon (1999), as the PDF of both the tracer and its gradient in the simulations eventually settles into a self-similar form wherein the width changes in proportion to the decay of standard deviation, but the shape remains invariant. The corresponding tracer pattern is sometimes referred to as a ''strange eigenmode'' (Pierrehumbert 1994) and is compatible with the assumptions made (though not justified) in Sinai and Yakhot (1989). In Pierrehumbert (2000) it was suggested that the discrepancy was due to limitations of the theory imposed by correlation-time assumptions, but a closer reading of Balkovsky and Fouxon (1999) shows that the prediction for the far tails is not subject to any such limits. The state of understanding of the problem is at present much in flux, but there are theoretical reasons Fereday et al. (2002) believe that the strange eigenmode behavior represents the correct long-term evolution, with the kind of evolution described in Balkovsky and Fouxon (1999) representing a transient, and possibly very limited, stage in the evolution.

Motivated by these recent studies, we inquire whether the aforementioned results can carry over to the more structured stratospheric flow, particularly in view of the existence of barriers to mixing, and to what extent the PDF of stratospheric tracer gradients can be understood in terms of concepts arising from theories for idealized flows. Examination of simulated tracer gradient PDFs is particularly important to progress, because the theory of these PDFs is much less complete than the corresponding theory for PDFs of the tracer itself. Further, the form of the gradient PDF is less universal (i.e., more sensitive to details of the advecting flow) than is the case for the tracer PDF (Balkovsky and Fouxon 1999). We address this issue by carrying out advection–diffusion simulations of a decaying passive tracer, driven by analyzed lower stratospheric winds [European Centre for Medium-Range Weather Forecasts (ECMWF) analyzed winds] on the 420-K isentropic surface using a high-resolution finite-volume model. Detailed information about the data source and the numerical model has been described in Part I.

Theoretical considerations on the PDF of tracer gradients are presented in section 2. Here we have recast the essential ideas of Balkovsky and Fouxon (1999) in a manner that draws out explicitly their implications for the shape of the gradient PDF in the decaying case. Our derivation also isolates the portion of the argument that is not subject to the uncertainties alluded to above. Simulation results on the PDFs of tracer gradients for realistic lower stratospheric flow are discussed in section 3, where the simulated PDFs are also compared with the PDFs of N_2O from the SKYHI model. A summary of our principal conclusions in the context of earlier work, together with some pointers to future work, is provided in section 4.

2. Theory of the gradient PDF for advection by smooth flow

a. Basic concepts

The problem of passive tracer mixing is governed by the advection–diffusion equation

$$\frac{\partial\theta}{\partial t} + \mathbf{v}\cdot\nabla\theta = \kappa\nabla^2\theta, \tag{1}$$

where θ indicates concentration or mixing ratio of a passive tracer; $\mathbf{v}$ is velocity, which satisfies the incompressible condition $\nabla\cdot\mathbf{v} = 0$ and the smoothness condition $|\nabla\mathbf{v}| < \infty$; and κ is diffusivity (molecular, numerical, or effective diffusivity). We study the problem of advection–diffusion in the limit of large Péclet number $\mathrm{Pe} = VL/\kappa \gg 1$. Here, V and L indicate velocity scale and its correlation length scale, respectively.

Multiplying (1) by θ and taking the space average gives

$$\frac{\partial\langle\theta^2\rangle}{\partial t} = -2\kappa\langle|\nabla\theta|^2\rangle. \tag{2}$$

Equation (2) means that the dissipation rate of a passive tracer is a function of the mean square of tracer gradients ($\nabla\theta$) for a given diffusivity κ. Thus, the problem of the statistics of tracer diffusive dissipation is reduced to the statistics of tracer gradients. The fluctuations of tracer gradients determine the degree of spatial intermittency of dissipation.

It can be easily shown that in the absence of diffusion the gradient PDF should be lognormal. Consider a tracer blob with initial size l_0 located at a point in an incompressible flow with Lyapunov exponent λ (assume λ is the positive Lyapunov exponent). After time t, the parcel has been stretched into a thin filament with length $l = l_0\exp(\lambda t)$ and width $r = l_0\exp(-\lambda t)$. Since there is no diffusion, tracer concentration tagged to a given fluid parcel does not change with time at all. Thus, the gradient associated with the tracer filament exponentially grows with time. Assume that the initial gradient near the blob is g_0; the gradient variation with time will be

$$g(t) = g_0\exp(\lambda t). \tag{3}$$

Here, g indicates the absolute value of the gradient; that is, $g = |\nabla\theta|$. Thus,

$$\lambda = \frac{1}{t}\ln\frac{g}{g_0}. \tag{4}$$

Based on generalizations of the central limit theorem, Chertkov et al. (1995) and Balkovsky and Fouxon (1999) showed that at long times the PDF of λ has the Gaussian form

$$P_\lambda(\lambda) \propto \exp\left[-\frac{(\lambda-\overline{\lambda})^2}{2\sigma_\lambda^2}\right], \tag{5}$$

with $\sigma_\lambda^2 \propto t^{-1}$. This form of the PDF is only valid if λ is not too far out on the tail of the distribution. On the far tails, Eq. (5) must be replaced by the *large deviation form*

$$P_\lambda(\lambda) \propto \exp[-t\Xi(\lambda-\overline{\lambda})], \tag{6}$$

where $\Xi(\zeta)$ is a nonuniversal function with a maximum at $\zeta = 0$; expanding in a Taylor series about $\zeta = 0$ recovers the Gaussian behavior in the core.

From Eq. (5) it follows that, in the core of the distribution, we have a lognormal PDF of the tracer gradients

$$P_g(t, g) \propto P_\lambda(\lambda) \propto \exp\left[-\frac{1}{at}(\ln(g) - \ln(g_0) - \overline{\lambda}t)^2\right], \tag{7}$$

where a is a parameter characterizing the standard deviation of tracer gradients. This argument is essentially the same as that given in Pierrehumbert and Yang (1993). Equation (7) shows that the lognormal distribution never reaches an equilibrium: its peak moves toward progressively higher gradients, while the width of the distribution increases. Without diffusion, there is nothing to halt the cascade of tracer variance to arbitrarily small scales. Additional results on the lognormal behavior of the gradient PDF can be found in Fouxon (1998). The far tails are not necessarily lognormal, and are governed by large-deviation theory.

b. *The tail of the gradient PDF in the presence of diffusion*

When diffusion is present, the situation is completely different. Our discussion in the following applies equally to the decaying tracer and forced equilibrium tracer cases. The filament arising from elongation of the tracer blob cannot be made infinitely thin, and therefore the tracer gradient does not grow exponentially. After time $t = 1/\lambda\ \ln(l_0/r_d)$, the straining process will be checked by diffusion so that there will be a quasi-steady balance between local strain and diffusion. Let r_d be the diffusive scale, that is, the smallest width scale the filament could sustain against diffusive dissipation. At the quasi steady state, the diffusive scale r_d can be determined by comparing the straining and diffusion terms in Eq. (1). The typical filament width, given by the most probably Lyapunov exponent, is thus

$$r_d^* = \sqrt{\frac{\kappa}{\overline{\lambda}}}. \tag{8}$$

Then, if $\delta\theta = \theta_1 - \theta_2$ is the typical concentration fluctuation (θ_1 and θ_2 being the concentration values at opposite sides of a filament), the typical gradient is $\delta\theta/r_d^*$.

From here, the argument leading to the PDF of the tracer gradients proceeds from estimating the gradient in terms of the typical fluctuation of the tracer across the filament, and the diffusive equilibrium width of the filament. If the concentration difference across a filament of thickness r is $\delta\theta$, the gradient at the quasi steady state is $g = |\nabla\theta| \approx \delta\theta/r$. Both $\delta\theta$ and r fluctuate in space and time, and the PDF of g must be derived in terms of the PDFs of its two ingredients. We will assume first that the values of θ on the two sides of the filament are uncorrelated, so that $P_{\delta\theta}(\delta\theta)$ is simply the convolution of the one-point tracer PDF $P(\theta)$ with itself. It is

easily shown that the large $\delta\theta$ tail of $P_{\delta\theta}$ has exactly the same form as the large θ tail of $P(\theta)$, though $P_{\delta\theta}$ will always look more Gaussian than $P(\theta)$ near its core. The second assumption we make, following Balkovsky and Fouxon (1999), is that the tracer fluctuation $\delta\theta$ is statistically independent of the filament thickness r. This is at first glance a surprising assumption to make, as it might have been thought that thin filaments would be associated with greater strain-induced diffusive decay and therefore systematically smaller $\delta\theta$. However, Balkovsky and Fouxon (1999) argue that the generation of anomalously large gradients proceeds via a process that decorrelates filament thickness and fluctuation amplitude. There are three measures of strain involved in the argument. The first is the instantaneous strain $\sigma(t)$, which is determined by the instantaneous velocity gradient matrix. The second is the strain $\Sigma(t)$ accumulated over a ''short'' averaging interval, whose span we will soon elucidate. The third is the Lyapunov exponent λ, which is a long-term accumulation of strain.

Long-term processes fill space with filaments decaying at the dominant scale r_d^*, and having various $\delta\theta$. These filaments provide the background of gradients of a ''typical'' magnitude. Large gradients arise when one of these filaments is subjected to an anomalously large short-term strain Σ, which *rapidly* strains the filament from r_d^* down to a smaller scale $r = \sqrt{\kappa/\Sigma} < r_d^*$. The straining happens so rapidly that $\delta\theta$ is preserved in the process, and thus remains independent of Σ. With the independence assumption, the gradient PDF is given by the convolution

$$P_g(g) = \int_{r=0}^{\infty} rP_{\delta\theta}(gr)P_r(r)\,dr. \tag{9}$$

If there were only a single filament scale $r = r_d^*$, then P_r would be a delta function concentrated at r_d^*, and hence the gradient PDF would have the same form as $P_{\delta\theta}$. In the actual case, we must obtain the form of $P_r(r)$.

The reason that the tail of the gradient PDF is sensitive only to short-term strain fluctuations is that anomalously large strain fluctuations that persist a long time lead to exponentially large enhancement of the decay rate of $\delta\theta$, wiping out the advantage of these fluctuations for creating large gradients. This remark also tells us what is meant by ''short term.'' For an instantaneous strain σ to cascade tracer down to a new dissipation scale requires a time of order $1/\sigma$. Hence, when we speak of short-term accumulation of strain, we mean accumulation over times comparable to the reciprocal of the typical strain rate. In the case where the instantaneous strain $\sigma(t)$ is a white-noise process in time (the so-called Kraichnan model), Balkovsky and Fouxon (1999) showed that P_r has the form

$$P_r(r) \propto \exp\left[-\left(\frac{r^*}{r}\right)^2\right], \tag{10}$$

where r^* is a coefficient determining the broadness of the distribution. The discussion in Balkovsky and Fouxon (1999) assumes that σ has a Gaussian distribution, but in fact it is easy to show for the Kraichnan model that the resulting finite-time strain PDF is independent of the form of the instantaneous strain PDF. It can be inferred from the derivation in appendix A of Balkovsky and Fouxon (1999) that r^* is on the order of $\sqrt{\kappa/\sigma_{\rm rms}}$, where $\sigma_{\rm rms}$ is the rms of the instantaneous strain. The derivation assumes that the ''typical'' strain has the same magnitude as its fluctuations about the typical value.

What happens if the instantaneous strain has finite correlation time? The PDF of the long-time Lyapunov exponents has a Gaussian core whose peak and width depend only on a few overall statistics of the advecting flow. This happy universality does not apply to the short-term strain PDF that determines P_r because a long correlation time makes it impossible for the filament to experience many independent strains in the time available, whence the central limit theorem never becomes applicable. It is only when the strain experienced by a parcel has a very short correlation time (relative to the strain rate itself) that the general form in Eq. (10) can be inferred. For example, if the instantaneous strain $\sigma(t)$ were very slowly varying, then the filament is in instantaneous strain–diffusive equilbrium, with $r(t) = \sqrt{\kappa/\sigma}$. In consequence, $P_r(r)$ would be determined by the shape of the PDF of the instantaneous strain. If the instantaneous strain had a Gaussian-tailed PDF, then Eq. (10) would be replaced by

$$P_r(r) \propto \exp\left[-\left(\frac{r^*}{r}\right)^4\right], \tag{11}$$

which proceeds from substituting $\sigma = \kappa/r^2$ into the Gaussian and then looking out onto the high-stretch (small r) tail. Alternately, if the strain has uniform probability for $-\sigma_m < \sigma < \sigma_m$ and zero probability other wise, then P_r has a sharp cutoff at $r = \sqrt{\kappa/\sigma_m}$, and therefore the tail of the gradient PDF P_g has exactly the same form as the tail of the concentration fluctuation PDF $P_{\delta\theta}$.

Suppose that $P_r(r) \propto \exp[-(r^*/r)^\beta]$ and $P_{\delta\theta}(\delta\theta) \propto \exp[-(\delta\theta/\sigma_\theta)^\alpha]$ on the low-probability tails of the distributions. Then by applying the steepest descent method to (9), it is found that the large g tail of the gradient PDF is given by

$$P_g(g) \propto \exp\left[-b\left(\frac{g}{g^*}\right)^\gamma\right], \tag{12}$$

where $g^* = \sigma_\theta/r^*$ is the typical gradient and

$$\gamma = \frac{\alpha\beta}{\alpha+\beta}, \qquad b = \left(\frac{\beta}{\alpha}\right)^{\alpha/(\alpha+\beta)} + \left(\frac{\alpha}{\beta}\right)^{\beta/(\alpha+\beta)}. \tag{13}$$

It follows from (13) that $\gamma < \alpha$. In other words, the gradient PDF always has fatter tails than the PDF of tracer fluctuations. This effect has been seen in the ide-

alized mixing simulations in Pierrehumbert (2000). The tails of the gradient PDF become fatter as $\beta \to 0$, since creation of very thin filaments by transient large strains becomes very probable in that limit. If the tracer PDF has typical exponential tails, and further, if the strain experienced by the filaments is rapidly fluctuating, then $\alpha = 1$ and $\beta = 2$, whence $\gamma = 2/3$. If the strain is slowly varying and has a Gaussian distribution, then instead we have $\beta = 4$ and $\gamma = 4/5$. In the so-called soft turbulence regime the concentration fluctuation itself is Gaussian (Castaing et al. 1989). In this case, $\alpha = 2$ and so the short-correlated strain yields exponential tails ($\gamma = 1$) of the gradient PDF. This behavior has been observed in the experiments of Thoroddsen and Van Atta (1992). Relations similar to (13) were also obtained by Bronski and McLaughlin (1999) and Bronski and McLaughlin (2000) in a very different approach.

The uncertainties concerning the long-term validity of the derivation given in Balkovsky and Fouxon (1999) revolve around the time evolution of the shape of the concentration PDF, and specifically the question of whether the shape ultimately becomes time invariant in the decaying case. If the concentration PDF (i.e., α) is known at any given time, then the corresponding gradient PDF can be inferred from the above arguments. If α becomes time independent, then the gradient PDF also attains a time-independent shape, though generally fatter-tailed than the concentration PDF.

c. A null hypothesis: Gradient PDFs for simple noise processes

Does a stretched exponential gradient PDF necessarily imply a dynamical process of the sort discussed above? As a test of a null hypothesis, we address in this section the question of whether stretched exponential behavior can emerge from simple unstructured noise processes.

Consider the family of 1D gradient fields

$$g(x) = \sum_{k=1}^{\infty} k^{-\zeta} A_j \sin[k(x - \phi_j)], \qquad (14)$$

where the ϕ_j are random phases and the A_j are random amplitudes uniformly distributed on the interval [0, 1]. The PDF for an ensemble of realizations is shown in Fig. 1 for various ζ. The case $\zeta = \infty$, equivalent to retaining only the first term in 14, shows a cusped behavior near the peak, which could be mistaken for a stretched exponential if one did not notice that the skirts do not extend very far out before being terminated by sharp shoulders. The best fit stretched exponential excluding the shoulders has $\gamma = 0.38$. The cusp has nothing to do with the arguments presented in the preceding section, and arises simply from the smoothness of the sin function near its peak. In fact, for an arbitrary function $f(x)$ with behavior $f = a - x^2$ near a maximum,

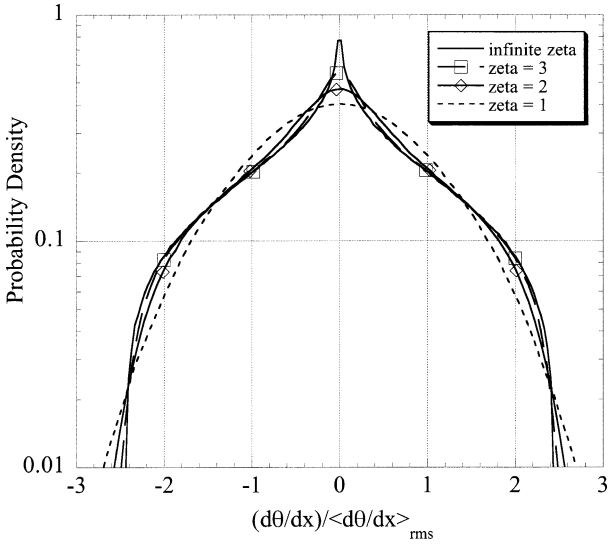

FIG. 1. PDFs for a sum of two random-phase sine waves, with and without contamination by red noise. The power spectrum of the noise is $k^{-2\zeta}$. See Eq. (14) for details.

the contribution to the PDF from the vicinity of the maximum is $P \propto 1./\sqrt{a - f}$, yielding a cusp.

The case $\zeta = 3$ is still strongly dominated by the first few modes, and the PDF is virtually identical to $\zeta = \infty$. As ζ decreases more modes come into play, and in accordance with the central limit theorem, the PDF becomes more Gaussian. The best fit stretched exponential has $\gamma = 1.06$ for $\zeta = 2$ and $\gamma = 1.92$ for $\zeta = 1$.

For $\zeta = 1$ the corresponding tracer field of which g is the gradient has a k^{-4} power spectrum. This still represents a very smooth tracer field—much smoother than the k^{-1} Batchelor spectrum proceeding from large-scale random advection, or the $k^{-5/3}$ spectrum proceeding from advection by Kolmogorov turbulence, or even the k^{-2} spectrum arising from a random arrangement of separated step discontinuities. A k^{-4} spectrum corresponds to a tracer field that is continuous, but has randomly arranged slope discontinuities. Bacmeister et al. (1996) found that stratospheric N_2O had a $k^{-5/3}$ power spectrum down to the smallest observable scales (somewhat below a kilometer). This corresponds to a gradient field with $\zeta = -1/6$ in the notation of Eq. (14). We have directly verified that the PDF appears Gaussian, as for the $\zeta = 1$ case, when 100 or more terms are included in the series. Thus, a random-phase noise field with the same power spectrum as the observed tracer field would yield a Gaussian gradient PDF. In contrast, the observed N_2O gradient PDF is stretched exponential (Hu 2000), indicating that the actual gradient field is much more structured than colored noise with the same spectrum.

We conclude that extensive stretched exponential tails—rather than just a cusped appearance near the peak—require that the tracer field result from a rather special sort of mixing process. The tails of the gradient PDF provide information about the dissipation scale and

the PDF of short-term strain. To extract this information, one also needs information about the form of the PDF of concentration fluctuations. The latter information can come either from observations or theory.

3. Simulation results

As in Part I, we study two classes of initial tracer conditions: ''zonal'' and ''meridional'' mixing. The initial conditions for the two cases are $\theta_0 = \cos(2x)$ and $\theta_0 = \cos(y)$, where x is longitude and y is latitude. In each case, we show the PDFs of zonal gradients ($\theta_x = \partial\theta/\partial x$), meridional gradients ($\theta_y = \partial\theta/\partial y$), and total gradients ($|\nabla\theta| = \sqrt{\theta_x^2 + \theta_y^2}$). Simulations are carried out using wind data from the same months as in Part I, July–August 1992. All the PDFs are calculated after a 2 month run (on 30 August). For the control runs, there is no explicit diffusion in the model, except for numerical diffusion.

a. Gradient PDFs in zonal mixing

Before we study the PDF of gradients, let us first look at the gradient fields. The plots in Fig. 2 show the maps of θ_x, θ_y, and $|\nabla\theta|$ for zonal mixing. The gradient field bears the clear imprint of the mean zonal jet structure, and of the degree of disturbance of the jets by planetary waves. The interplay of jets and waves results in the substantial interhemispheric asymmetry evident in the figures.

In the northern surf zone (roughly from the equator to 45°N) the tropical easterlies and midlatitude westerlies result in a series of high-gradient regions concentrated on filaments angled about 20°–30° to the latitude circles. These filaments are largely associated with wave breaking events in the surf zone. Some high-gradient filaments extend into the arctic regions, though they are more contorted there. This results from substantial lower stratospheric planetary wave activity in the Northern Hemisphere. High-gradient filaments also extend somewhat south of the equator, into the southern surf zone. The filaments are highly contorted there, because there is little mean shear to organize the pattern. South of 45°S, the gradients are weak and concentrated on zonally oriented streaks. This pattern arises from the strong and unperturbed Antarctic winter vortex. The long zonal filaments near the South Pole mark the polar mixing barrier surrounding the Antarctic polar vortex.

The field of meridional gradient θ_y (Fig. 2b) has much larger fluctuations than that of the zonal gradient field θ_x (Fig. 2a). This is because zonal wind shear always tends to smooth out zonal tracer variations and to orient tracer structures zonally. As a result, the total gradient field $|\nabla\theta|$ (Fig. 2c) has a similar pattern to the meridional gradient field.

We have examined the time evolution of moments of the gradient field. During the first 8 days, the moments grow; this is the stage during which the strain is cascading tracer variance down to the dissipation scale, before which there is little diffusive dissipation. Following the transient stage, all moments we were able to reliably compute decay according to the law

$$\langle |\nabla\theta|^n \rangle = A_n \exp(-\Gamma_n t), \tag{15}$$

where Γ_n indicates the decay rate. Figure 3 shows the behavior of Γ_n as a function of n. Comparing to Fig. 7 of Part I, we find that the decay rates for the gradient field are nearly the same as those for the tracer field itself. This behavior is consistent with the predictions of Balkovsky and Fouxon (1999). The reasoning behind this result is simple. Because there is no correlation between dissipation scale r and the tracer fluctuation $\delta\theta$, and because the PDF of r attains an equilibrium shape, the dissipation rate of a gradient fluctuation is determined only by the magnitude of the concentration fluctuation in the corresponding filament. There is no tendency, say, for large amplitude fluctuations to have systematically smaller dissipation scales. Although the Γ_n are the same for the tracer decay and gradient decay, the prefactors A_n need not be the same; indeed they are generally different, since gradient PDFs typically have fatter tails (more stretched exponential) than the exponential tails of tracer PDFs. For the reasons discussed in Part I, the flattening of the Γ_n curve implies that the gradient and the concentration PDFs are not self-similar in time, but rather evolve toward progressively fatter tails as time goes on. This evolution is peculiar to the decaying case, and has no counterpart in equilibrium problems where the tracer variance is maintained by a source. There are reasons to suspect that the evolution of the shape represents a transient stage, which ultimately gives way to strange eigenmode behavior in which the shape stops evolving [cf. the numerical results in Pierrehumbert (2000)]. Fereday et al. (2002) have provided a clear counterexample to the prediction of Balkovsky and Fouxon (1999), and have discussed the processes governing the long-term self-similar decay of the tracer fluctuations. It is not yet know what factors determine the length of time for which the behavior in Balkovsky and Fouxon (1999) applies.

Figure 4 shows the PDFs of θ_x, θ_y, and $|\nabla\theta|$ [denoted by grad(θ) in the figure] for zonal mixing, respectively. The vertical axis is logarithmic, and the gradients are all normalized by their respective rms. The PDFs of θ_x (Fig. 4a) and θ_y (Fig. 4b) all show concave shapes with sharp cuspy peaks. The PDF of total gradient $|\nabla\theta|$ can be well fitted by a stretched exponential curve, with a stretching parameter $\gamma \approx 0.56$ (Fig. 4c). The fitting curve (dotted line) is almost overlapped by the PDF curve (solid line). Note that the stretched exponential curve does not fit the peak of the PDF, where the PDF shows a Gaussian-like core for small gradients. The width of this range is about 0.0–0.3.

Note that the stretched exponential tails extend to out to nine standard deviations, yielding a decay in probability of four orders of magnitude. The very extensive

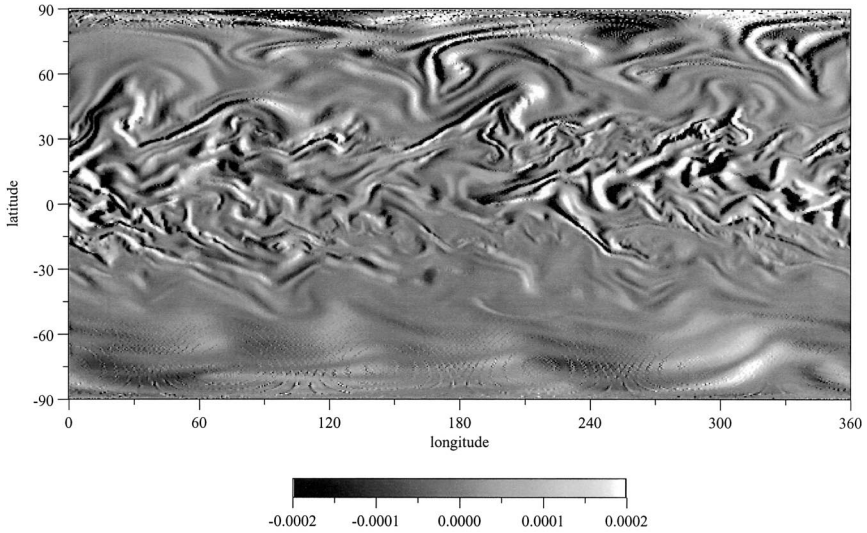
90
60
30
0
-30
-60
-90
latitude
0
60
120
180
240
300
360
longitude
-0.0002
-0.0001
0.0000
0.0001
0.0002

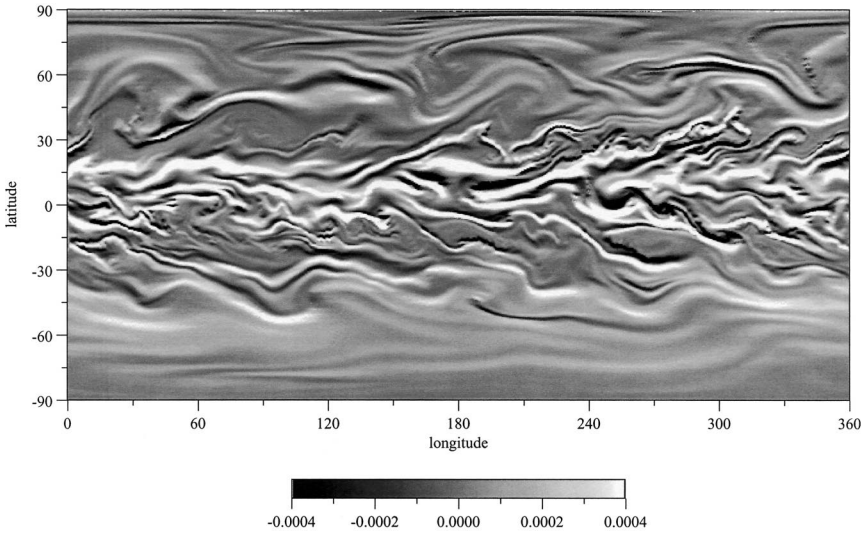
90
60
30
0
-30
-60
-90
latitude
0
60
120
180
240
300
360
longitude
-0.0004
-0.0002
0.0000
0.0002
0.0004

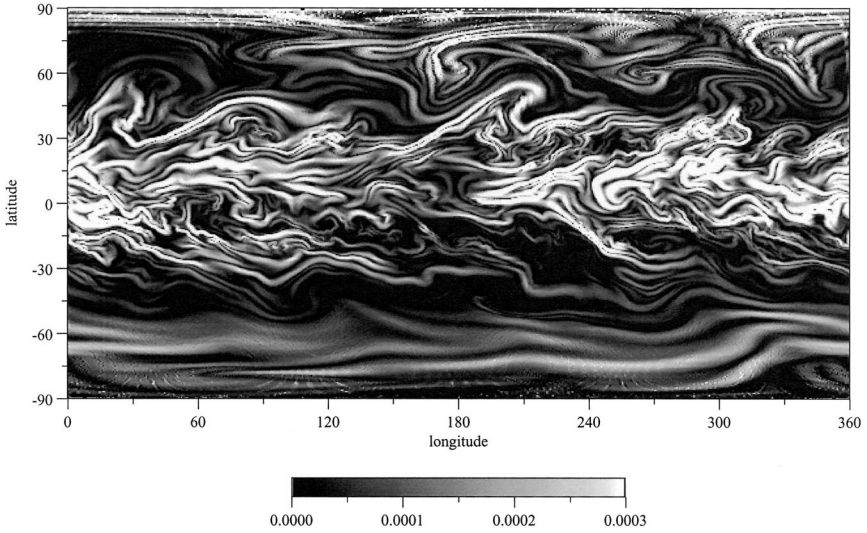
90
60
30
0
-30
-60
-90
latitude
0
60
120
180
240
300
360
longitude
0.0000
0.0001
0.0002
0.0003

scaling range proves that a wide range of strains have acted to produce a diverse population of anomalously thin filaments. The behavior captured by the PDF is very different from the sort arising from gradients of smooth noise processes, exemplified by Fig. 1. The extensive scaling range seen in Fig. 4 is typical of all the simulated gradient PDFs we shall encounter, so we shall not call attention to it in every instance.

In order to distinguish the stretched exponential PDF from lognormal distributions, the curves in Fig. 4c are replotted, together with a lognormal fitting curve, in Fig. 5 in a log–log form. Neither curve fits the PDF near the peak. The lognormal curve fits the PDF only in the range $0.1 \geq |\nabla\theta|/|\nabla\theta|_{\text{rms}} \leq 1.1$, which is near to the Gaussian-like core. For large gradients, the lognormal curve largely deviates from the PDF, while the stretched exponential curve fits the PDF tail very well.

Figure 6 shows the PDFs of θ_x separately for both hemispheres. They quantify the hemispheric differences that are evident to the eye in the gradient maps, Fig. 2. The PDF in the Northern Hemisphere (Fig. 6a) has broader tails than that in the Southern Hemisphere (Fig. 6b). The PDFs of θ_y in Fig. 7 show even more significant differences between the two hemispheres. The Southern Hemisphere PDF has shoulders reminiscent of those in Fig. 1, indicative of a sharp cutoff at high strains, and perhaps also of long-correlated strain behavior. The PDF also exhibits some skewness, which is not accounted for by any of the theoretical considerations discussed above. Since the initial condition is symmetric between positive and negative values of the concentration fluctuation, the skewness is an artifact of the particular choice of phase of the initial condition relative to the location of trapping regions in the Tropics. Reversing the sign of the initial condition, for example, would reverse the sense of the skewness. We therefore do not think that much general significance can be attached to the skewness appearing in the zonal mixing case.

The interhemispheric asymmetry provides an interesting case study regarding the manner in which fluctuations in long-term strain (the Lyapunov exponents) enter into the creation of anomalously large gradients. The Southern Hemisphere gradients are generally weak, though one might have expected large gradients there because the generally larger Lyapunov exponents (see Part I) should create small scales. This does not happen because the large long-term strain in fact leads to a strengthened exponential decay of tracer fluctuation, so that $\delta\theta$ is smaller in the Southern Hemisphere than in the Northern Hemisphere. The large gradients appear in the northern surf zone, which is not an area of particularly large Lyapunov exponents. They appear there because filaments with large $\delta\theta$ are frequently swept into the strongly sheared jet in the surf zone, where they experience short-term strain fluctuations that quickly amplify the gradient.

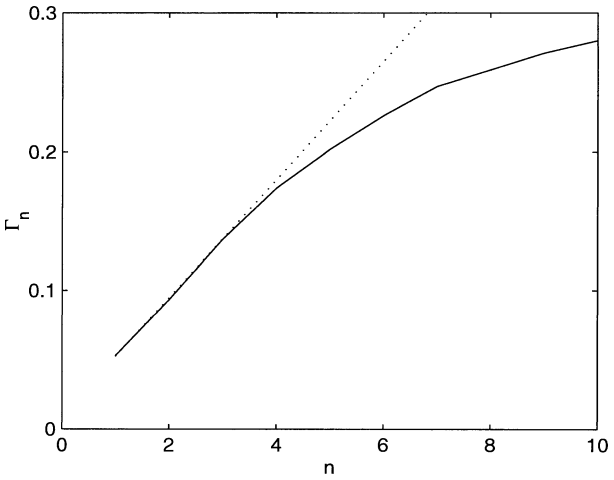

FIG. 3. Decay rate Γ_n as a function of moment order n.

In Part I, we showed that the PDF of the tracer concentration is nearly exponential ($\alpha \approx 1$) at the later stages of the evolution. From (13), the computed value $\gamma \approx 0.56$ implies a strain parameter $\beta \approx 1.27$. This is considerably less than the value corresponding to δ-correlated strain, but since the stratospheric flow evolves slowly in time, there is no good reason to expect the strain to have short correlation time. What is interesting is that the indicated value of β indicates a higher probability of very thin filaments than would be obtained from δ-correlated strain. Such behavior could be obtained from persistent strain, but only if the PDF of the instantaneous strain itself were very fat-tailed; Gaussian persistent strain yields $\beta = 4$. Further insight is gained by examining the gradient PDFs in the two hemispheres separately. In the Northern Hemisphere, the tracer concentration PDF (see Fig. 9a in Part I) has a stretching parameter $\alpha \approx 0.9$. Combining it with $\gamma \approx 0.56$ (Fig. 4a) yields $\beta \approx 1.5$. In the Southern Hemisphere, using $\alpha \approx 1.2$ (see the right tail in Fig. 9b of Part I) and $\gamma \approx 0.85$ (the combination of Figs. 6b and 7b) gives $\beta \approx 3.6$. The Northern Hemisphere behavior is thus similar to that revealed by the global PDF (whose behavior is dominated by the large Northern Hemisphere gradients). The Southern Hemisphere, in contrast, is more compatible with persistent, Gaussian-distributed strain.

b. Gradient PDFs in meridional mixing

The gradient fields for the case of meridional mixing are shown in Fig. 8. Large gradients mainly occur in

←

FIG. 2. Gradient maps for zonal mixing after day 60 (30 August 1992): (a) zonal gradient (θ_x), (b) meridional gradient (θ_y), and (c) total gradient ($|\nabla\theta|$).

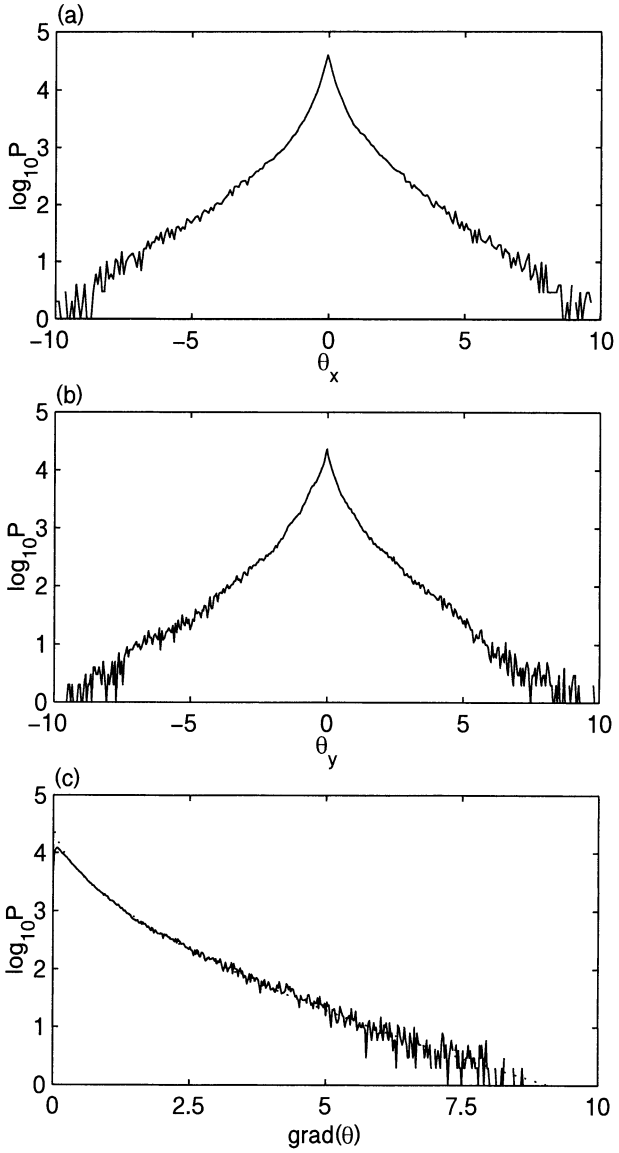

FIG. 4. Gradient PDFs for zonal mixing after day 60 (30 August 1992): (a) $P(\theta_x)$, (b) $P(\theta_y)$, and (c) $P(|\nabla\theta|)$. The dotted line in (c) is a stretched exponential fitting curve with stretching parameter $\gamma \approx 0.56$.

the Northern Hemisphere. The lack of large gradients in the Tropics is because the initial condition $\cos(y)$ remains less mixed. As in the zonal mixing case, in the Northern Hemisphere gradient filaments also show southwest–northeast orientation, while the filaments are zonally oriented in the Southern Hemisphere. Again, a long gradient filament near the South Pole marks the polar mixing barrier. In Part I, it was found that, owing to mixing barriers, the moments of the concentration fluctuation decay little with time. Consistently with this result, we find that the gradient moments for meridional mixing also show little decay (figure not shown). Because of the persistent global background gradient, the meridional mixing case is expected to behave qualitatively like a case in which the background tracer gradient is maintained by sources and sinks.

Figure 9 shows the gradient PDFs in meridional mixing. These PDFs are similar to that in zonal mixing, with dominant stretched exponential tails. The PDF of total gradients ($|\nabla\theta|$) can be fitted by a stretched exponential curve, with a stretching parameter $\gamma \approx 0.55$ (Fig. 9c). The Gaussian-like core and the blowup of the fit near the PDF peak can also be seen.

Figure 10 shows the PDFs of θ_x in the Northern and Southern Hemispheres, and the corresponding results for θ_y are shown in Fig. 11. The PDF in the Northern Hemisphere is much broader than that in the Southern Hemisphere, largely because the tracer fluctuations are weaker in the Southern Hemisphere. This hemispheric asymmetry is even more pronounced than was the case for zonal mixing, presumably because the weak Southern Hemisphere planetary waves are inefficient at creating tracer fluctuations from the background meridional gradient. A striking feature is the pronounced skewness in the PDF of θ_y, which primarily arises in the Northern Hemisphere. Large negative gradients are considerably more probable than large positive gradients. Evidently, as tongues of tropical air bearing high tracer values are extruded into the northern surf zone, their poleward flanks experience systematically greater strain than the equatorward flanks.

It is interesting to compare the gradient PDFs in meridional mixing with that of N_2O in the SKYHI model with horizontal resolution of $1° \times 1.25°$ in latitude–longitude grids, since N_2O has a background profile that is generally high in the tropical source region and low in the polar regions which are flushed by N_2O-depleted upper stratospheric air. Because the diabatic sinking that accomplishes this flushing has a pronounced seasonal cycle, N_2O will exhibit some features that are not present in the simpler meridional mixing experiment. Nonetheless, some points of similarity between the N_2O and the meridional mixing PDFs can be seen. The data used here are from 30 August 1983 (model time). Figure 12 shows the gradient PDFs of N_2O on the 450-K isentropic surface, which is slightly higher than that in our simulations, 420 K. Comparison of this figure with Fig. 9 shows several similarities, with an almost symmetric PDF of $[N_2O]_x$, and skew PDF of $[N_2O]_y$. In the tails the stretching parameter for the PDF of total gradients is about 0.56. Differences are also obvious. First, the PDF of $[N_2O]_y$ shows more pronounced skewness than that in our simulations. Second, the PDFs of N_2O gradients in the SKYHI model show larger Gaussian-like cores and shorter tails. Further, the N_2O gradient PDFs show sharp shoulders terminating the tails. This is symptomatic of limited resolution in the model, which truncates the scales (and perhaps also the strains), which would give rise to the higher gradients.

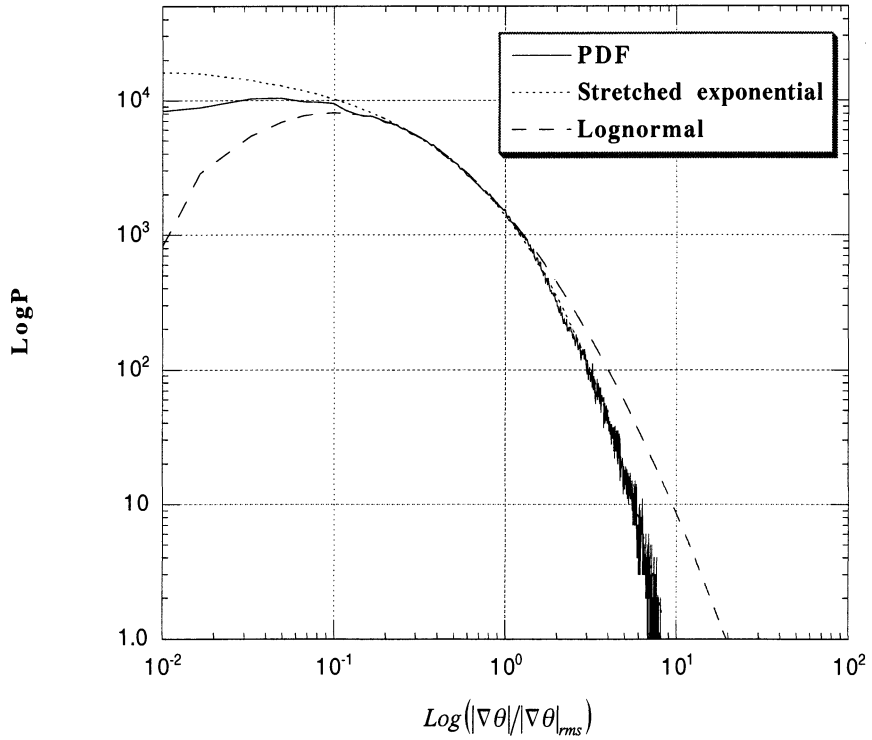

FIG. 5. Comparison of a stretched exponential fit (dotted line) with a lognormal fit (dashed line). The PDF curve is same as that in Fig. 4c, but in log–log plot.

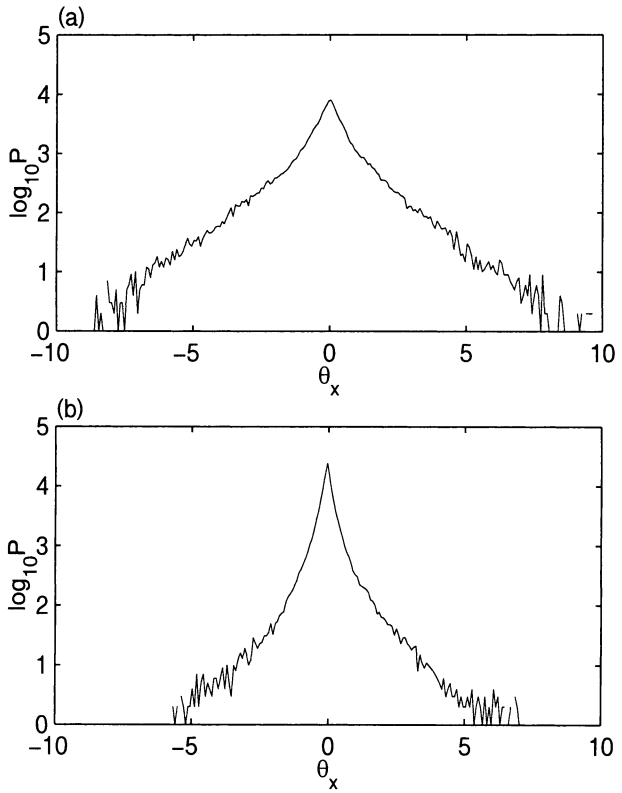

FIG. 6. PDFs of θ_x in zonal mixing: (a) Northern Hemisphere and (b) Southern Hemisphere.

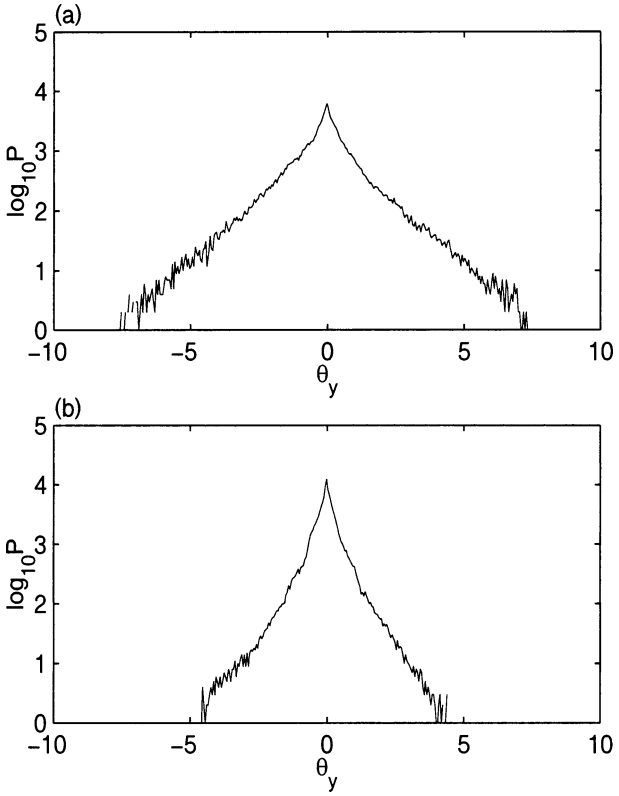

FIG. 7. PDFs of θ_y in zonal mixing: (a) Northern Hemisphere and (b) Southern Hemisphere.

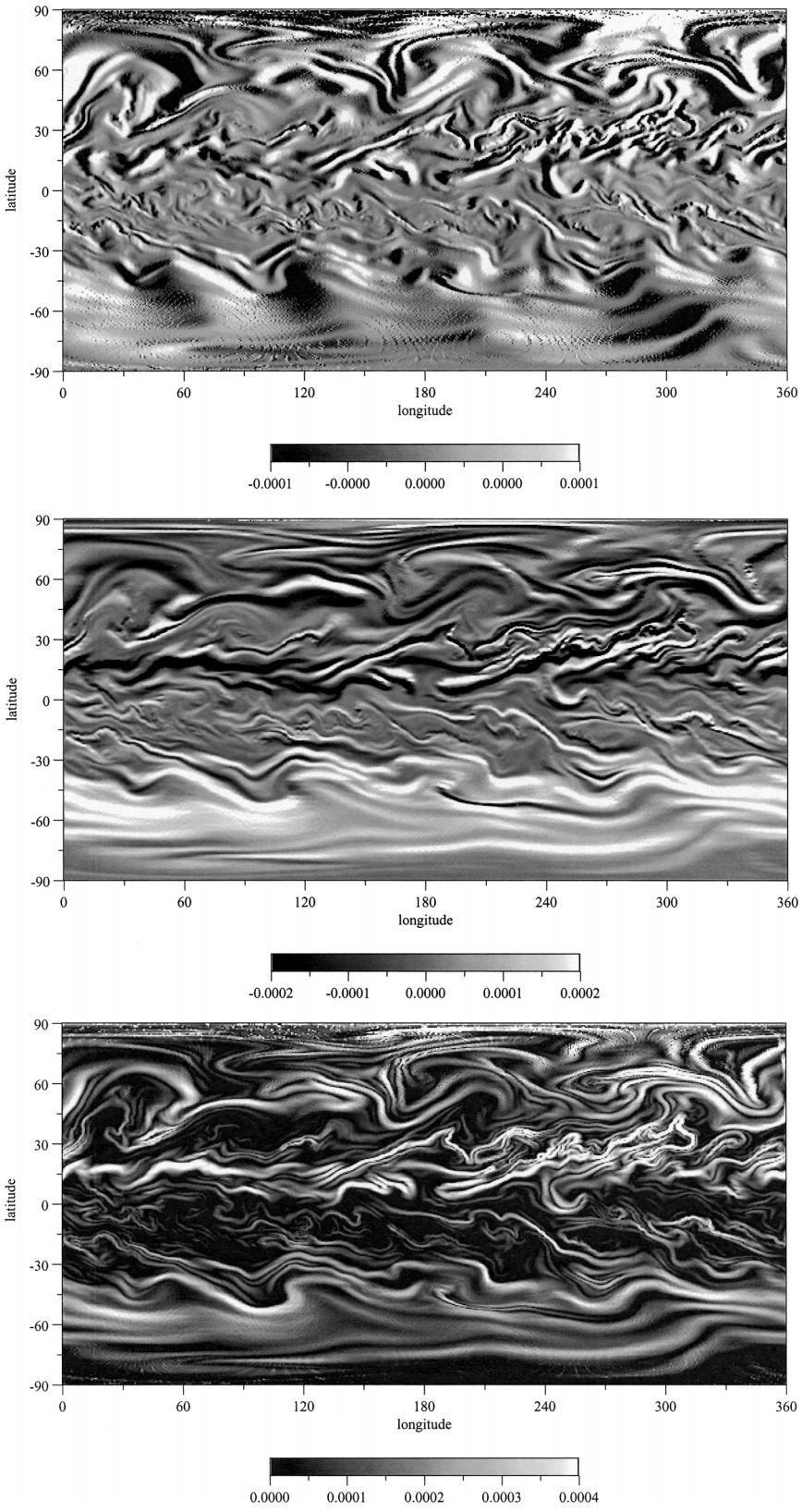
90
60
30
0
-30
-60
-90
latitude
0
60
120
180
240
300
360
longitude
-0.0001
-0.0000
0.0000
0.0000
0.0001
90
60
30
0
-30
-60
-90
latitude
0
60
120
180
240
300
360
longitude
-0.0002
-0.0001
0.0000
0.0001
0.0002
90
60
30
0
-30
-60
-90
latitude
0
60
120
180
240
300
360
longitude
0.0000
0.0001
0.0002
0.0003
0.0004

c. Diffusivity effect on the PDF of gradients

In section 2 it was shown that the parameters of the stretched exponential tail of the gradient PDF are independent of the magnitude of the diffusivity. We test this issue by adding an explicit diffusion term to the model, and inquire as to whether there are other aspects of the shape of the PDF that do depend on the magnitude of the diffusivity.

Figure 13 shows the PDFs of zonal gradients $P(\theta_x)$ in the case of zonal mixing with different diffusivities: $\kappa = 1.0 \times 10^5$, 2.0×10^5, and 3.0×10^5 m^2 s^{-1}. As diffusivity increases, skirts occur at the ends of the PDF curves, and the valid range of the stretched exponential fitting curve becomes shorter. The same behavior is also found for the PDF of meridional gradients (figure not shown). The steep shoulders that terminate the stretched exponential range resemble those encountered for very smooth functions in Fig. 1. The cutoff point can be determined by

$$g_{\max} = \theta_{\text{rms}} \sqrt{\frac{\Sigma_{\max}}{\kappa}}, \tag{16}$$

because the width of tracer filaments cannot be less than $r = \sqrt{\kappa/\Sigma_{\max}}$, where $\Sigma_{\max}$ is the maximum short-term accumulated strain of the advecting flow. Thus, the theoretical prediction of the stretched exponential PDF is valid only for the range $g < g_{\max}$. A larger diffusivity κ leads to a greater scale r and consequently a smaller $g_{\max}$. In other words, larger diffusivity cuts off more of the stretched exponential tails. This is also why the PDFs of N_2O in the SKYHI model have short stretched exponential tails. Overall, change of diffusivity leads to a change of the range of stretched exponential distribution, but does not change the stretched exponential property.

Note that the appearance of shoulders in the gradient PDF signals the existence of a maximum strain $\Sigma_{\max}$. If the strain were in fact unbounded, then changing the diffusivity would change the width of the distribution through changing g^* in Eq. (12), but it would not change the shape of the distribution. The reason is that infrequent large strains would still create arbitrarily small r, so there would be no sharp gradient cutoff. Shoulders were not seen in our weakly diffused calculation (e.g., Fig. 4) because $g_{\max}$ was so large that its probability of occurence was small and the shoulders were lost in statistical noise. With larger diffusivity, the cutoff has moved to scales where it can be resolved.

The preceding discussion underscores that, via the PDF, one can detect the influence of diffusivity on the tracer field even if one does not actually detect the minimum scale present in the tracer field. This is a consequence of the broad range of strain, leading to a broad range of dissipation scales. The stretched exponential PDF, and its exponent, directly reflect the action of dissipation. It is not necessary to see the shoulders of the PDF in order to draw useful inferences about the nature of the dissipation.

It is also interesting that the introduction of explicit ∇^2 diffusivity, which swamps the numerical diffusivity

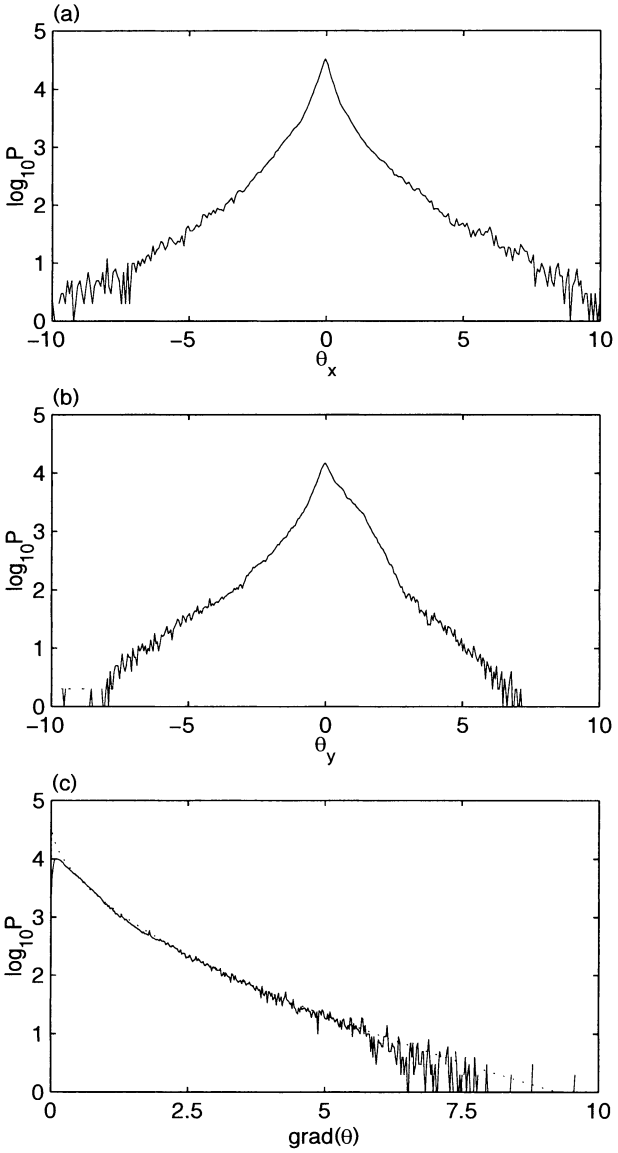

FIG. 9. Gradient PDFs for meridional mixing after day 60 (30 August 1992): (a) $P(\theta_x)$, (b) $P(\theta_y)$, and (c) $P(|\nabla\theta|)$. The dotted line in (c) is a stretched exponential fitting curve with stretching parameter $\gamma \approx 0.55$.

←

FIG. 8. Gradient maps for meridional mixing after day 60 (30 August 1992): (a) zonal gradient (θ_x), (b) meridional gradient (θ_y), and (c) total gradient ($|\nabla\theta|$).

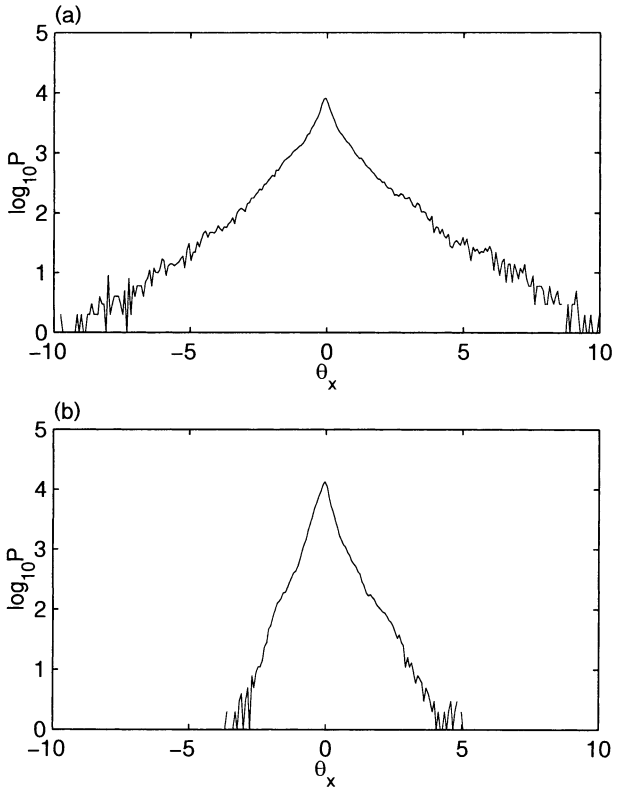

FIG. 10. PDFs of θ_x in meridional mixing: (a) Northern Hemisphere and (b) Southern Hemisphere.

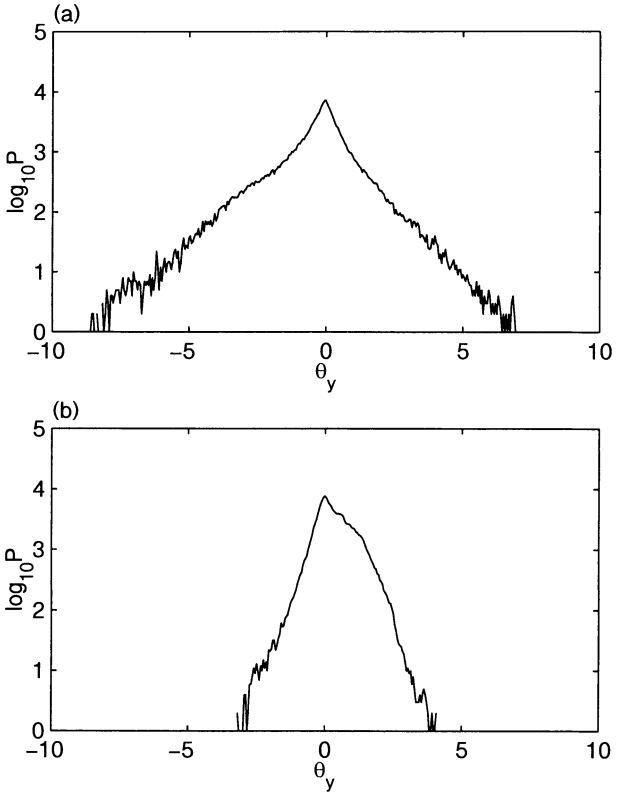

FIG. 11. PDFs of θ_y in meridional mixing: (a) Northern Hemisphere and (b) Southern Hemisphere.

of the Van Leer scheme, does not change the shape of the PDF, apart from the introduction of shoulders at the cutoff. Since the shape of the PDF is, as we have argued above, somewhat sensitive to the scale selectivity of the dissipation, through its effect on P_r, one needs to be concerned about whether the simulated gradient results are sensitive to unphysical aspects of the numerical diffusivity. The implicit diffusivity of the Van Leer scheme is evidently close enough to Newtonian diffusivity at small scales that this issue is not too serious.

4. Discussion and conclusions

We have argued that advection–diffusion by a broad class of lower stratospheric flows should produce a stretched exponential probability distribution function (PDF) of tracer gradients. This results from a joint effect of dissipation and short-term strain fluctuations; the gradient PDF is not simply the lognormal distribution expected in the undiffused case, with tails truncated by diffusion. The deviation occurs because dissipation affects the statistics of the dissipation length in a rather subtle way. One cannot get the right answer by doing inviscid straining and bringing in diffusion afterward, as the actions of diffusion and straining do not commute. Our statistical work thus goes beyond the treatment in Haynes and Anglade (1997), who to some extent relied on undiffused strain statistics to estimate the fluctuation of scales.

Simulations show that the theoretical expectations are borne out even for realistic stratospheric advection. We have discussed simulations only for the case of a decaying tracer, but the theoretical arguments relating the gradient PDF to the tracer PDF are independent of whether the tracer is decaying or maintained. The tracer PDF has different long-term behavior in the decaying versus maintained case, but the gradient PDF is generally expected to be fatter-tailed than the tracer PDF itself. Moreover, in the case of mixing of an initially meridional large-scale gradient, the background gradient decays little over the course of the integration, and so the evolution is very similar to what one would obtain if the large-scale gradient were maintained by a source–sink distribution. For both meridional and zonal mixing, we find that the gradient PDF is stretched exponential, with stretching parameters of $\gamma \approx 0.56$. The theoretical expectation for γ depends on the shape of the PDF of short-term strain. This quantity is very problem dependent, and we have shown that it varies considerably between the Northern (summer) and Southern (winter) Hemispheres. The short-term strain PDF can be diagnosed for a given flow, but unless the instantaneous strain has very short time correlations, there is essen-

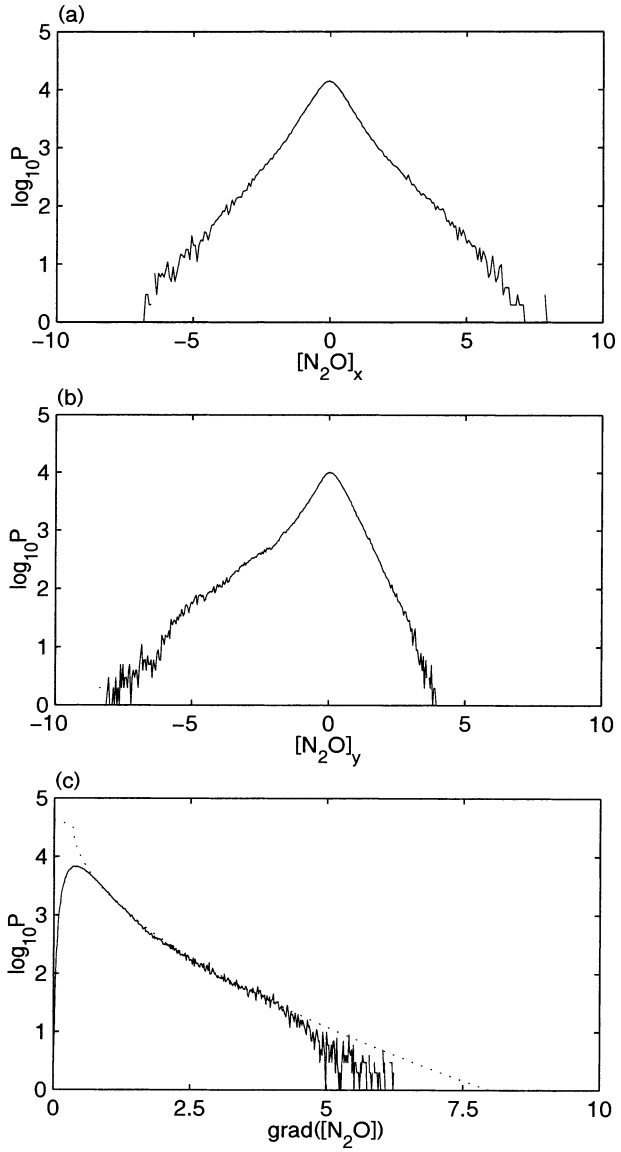

FIG. 12. Gradient PDF of N_2O in the SKYHI model (30 August 1983): (a) $P([N_2O]_x)$, (b) $P([N_2O]_y)$, and (c) $P(|\nabla[N_2O]|)$. The dotted line in (c) is a stretched exponential fitting curve with stretching parameter $\gamma \approx 0.56$.

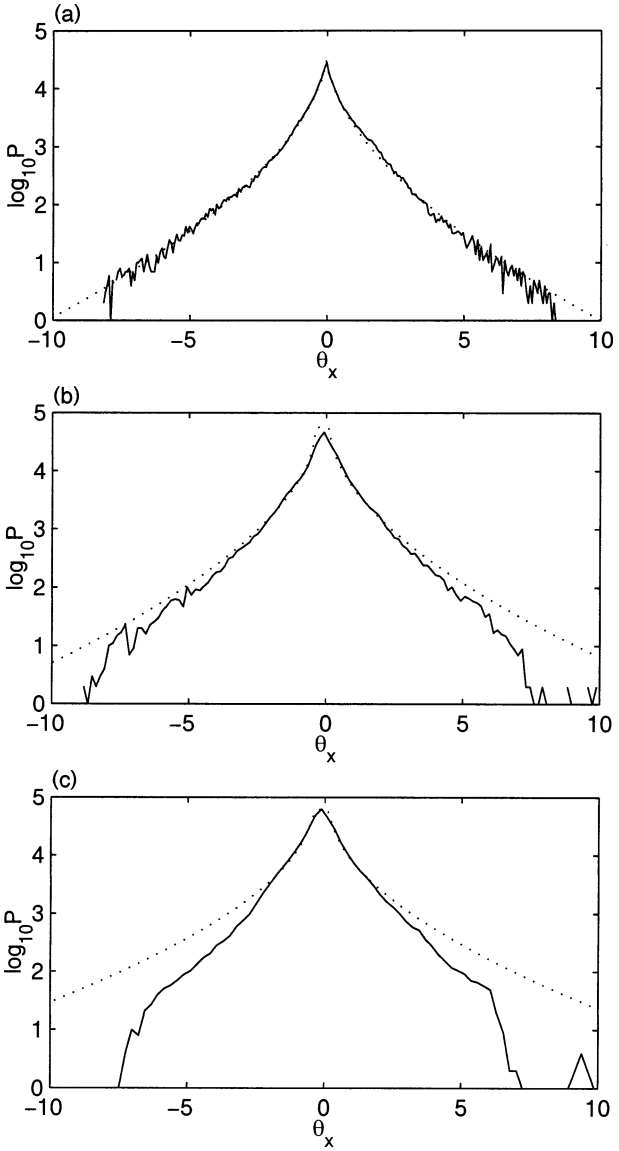

FIG. 13. $P(\theta_x)$ in zonal mixing with different diffusivity: (a) $\kappa = 1.0 \times 10^5$ m^2 s^{-1}, (b) $\kappa = 2.0 \times 10^5$ m^2 s^{-1}, and (c) $\kappa = 3.0 \times 10^5$ m^2 s^{-1}. The dotted lines are stretched exponential fitting curves with the same stretching parameter $\gamma \approx 0.56$ and different b.

tially no theoretical guidance as to what PDF one should expect.

Regarding regional patterns, we found also that the largest gradient fluctuations are not found in the regions of largest Lyapunov exponents, because the large long-term strain leads to rapid dissipation and small values of tracer fluctuations there. Rather, the largest gradients appear where the tropical pool of large undamped tracer fluctuations are processed in the high-strain region of the surf zones.

The gradient PDF is sensitive to the presence of dissipation, and its width is determined by the mean dissipation scale r^*. However, one should not expect the power spectrum to show a sharp rolloff at r^*, since there is not in fact a unique dissipation scale. Rather, there is a range of dissipation scales corresponding to the fluctuation of short-term strains (Antonsen et al. 1996; Yuan et al. 2000). This is why observed tracer PDFs (Hu 2000; Sparling and Bacmeister 2001) show the stretched exponential form characteristic of dissipation, despite the fact that power spectra show no short-wave rolloff (Strahan and Mahlman 1994; Bacmeister et al. 1996). We have shown that the appearance of a stretched exponential in the gradient PDF over two or more orders of magnitude of decay of probability is highly significant. It cannot be obtained by generic ran-

dom processes. For example, a random-phase Fourier series with the same $k^{-5/3}$ power spectrum as the observed N_2O field yields a Gaussian gradient PDF rather than stretched exponentials. Thus, the gradient PDF truly contains information about the tracer variability structure that is not present in the power spectrum alone.

The gradient PDF is a good object for observational analysis and model data comparison. Extensive stretched exponential tails are evidence of the action of dissipation, and are even sensitive to the scale selectivity of the dissipation. For example, Newtonian ∇^2 diffusion yields a different stretching exponent than ∇^4 hyperdiffusion, because ∇^4 would produce a P_r that decays more rapidly at small r than is the case for ∇^2, all other things being equal. A transition between the first and second law at intermediate scales would show up in the gradient PDF as a kink in the tail at intermediate gradients. The appearance of a sharp cutoff or ''shoulders'' in the PDF at large gradients is indicative of a combination of large dissipation and a sharp cutoff of the high-stretch tail of the strain PDF. Shoulders can also appear if the diffusion law becomes extremely scale selective at small scales. At present, the inferences concerning the role of the dissipation law are rather speculative, and the suggested behavior remains to be verified by appropriate simulations.

The skewness we have found in the meridional gradients in the presence of a mean meridional gradient is not accounted for by any of the homogeneous isotropic theories. This skewness is physically important, as it implies a preferred direction of diffusive transport relative to the mean background gradient. Theoretical inquiries as to the nature of the skewness would be a fruitful avenue for future work.

In addition, our simulations have been purely two-dimensional, balancing two-dimensional strain on an isentropic surface against horizontal diffusion. In the spirit of Haynes and Anglade (1997), the all-important vertical diffusion effects are reflected in our results through an effective (and greatly enhanced) horizontal diffusivity. However, since the effective horizontal diffusivity is sensitive to the statistics of the vertical shear in the advecting flow, a comprehensive treatment of gradient statistics should take into account the observed fluctuations in vertical shear. Haynes and Anglade (1997) evaluate the vertical-scale cascade statistics in a purely nondiffused model, but we expect that the mutual effects of diffusion and strain would produce significantly different statistics of the vertical gradients, just as we have shown to be the case for horizontal gradients. Since only the local vertical shear is of interest, there are possibilities for carrying out such a calculation without resorting to fully three-dimensional simulations. This approach will be pursued in future work.

Acknowledgments. We are grateful to Eugeni Balkovsky and Alexander Fouxon for helpful discussion on the theoretical issues. We thank Richard Wardle, Jai Sukhatme, and Doug Allen who provided us with many useful suggestions. We also thank Rich McLaughlin and Jared Bronski whose work has greatly inspired us. This work was supported by the National Science Foundation under Grant ATM9505190 and the ASCI Flash Center at the University of Chicago under DOE Contract B341495.

REFERENCES

Antonsen, T. M., Z. Fan, E. Ott, and E. Garcia-Lopez, 1996: The role of chaotic orbits in the determination of power spectra of passive scalars. *Phys. Fluids,* **8,** 3094–3104.

Bacmeister, J. T., and Coauthors, 1996: Stratospheric horizontal wavenumber spectra of winds, potential temperature, and atmospheric tracers observed by high-altitude aircraft. *J. Geophys. Res.,* **101,** 9441–9470.

Balkovsky, E., and G. Falkovich, 1998: Two complementary descriptions of intermittency. *Phys. Rev.,* **57E,** 1234–1234.

——, and A. Fouxon, 1999: Universal long-time properties of Lagrangian statistics in the Batchelor regime and their application to the passive scalar problem. *Phys. Rev.,* **60E,** 4164–4174.

Balluch, M. G., and P. H. Haynes, 1997: Quantification of lower stratospheric mixing processes using aircraft data. *J. Geophys. Res.,* **102,** 23 487–23 504.

Bronski, J. C., and R. M. McLaughlin, 1999: The problem of moments and the Majda model for scalar intermittency. *Phys. Lett.,* **265A,** 257–263.

——, and ——, 2000: Rigorous estimates of the tails of the probability distribution function for the random linear shear model. *J. Stat. Phys.,* **98,** 897–915.

Castaing, B., and Coauthors, 1989: Scaling of hard thermal turbulence in Rayleigh–Benard convection. *J. Fluid Mech.,* **204,** 1–30.

Chertkov, M., G. Falkovich, I. Kolokolov, and I. Lebedev, 1995: Statistics of a passive scalar advected by a large-scale two-dimensional velocity field: Analytic solution. *Phys. Rev.,* **51E,** 5609–5627.

——, ——, and ——, 1998: Intermittent dissipation of a passive scalar in turbulence. *Phys. Rev. Lett.,* **80,** 2121–2125.

Fereday, D. R., P. H. Haynes, A. Wonhas, and J. C. Vassilicos, 2002: Scalar variance decay in chaotic advection and Batchelor-regime turbulence. *Phys. Rev.,* **65E,** 03501-1–03501-4.

Fouxon, A., 1998: Evolution of a scalar gradient's probability density function in a random flow. *Phys. Rev.,* **58E,** 4019–4022.

Gurvich, A. S., and A. M. Yaglom, 1967: Breakdown of eddies and probability distributions for small-scale turbulence. *Phys. Fluids,* **10,** 559–565.

Haynes, P. H., and J. Anglade, 1997: The vertical-scale cascade in atmospheric tracers due to large-scale differential advection. *J. Atmos. Sci.,* **54,** 1121–1136.

Hu, Y., 2000: The advection–diffusion problem for stratospheric flow. Ph.D. thesis, University of Chicago, 268 pp.

——, and R. T. Pierrehumbert, 2001: The advection–diffusion problem for stratospheric flow. Part I: Concentration probability distribution function. *J. Atmos. Sci.,* **58,** 1493–1510.

Kraichnan, R. H., 1974: Convection of a passive scalar by a quasi-uniform random strain field. *J. Fluid Mech.,* **64,** 737–762.

Pierrehumbert, R. T., 1994: Tracer microstructure in the large-eddy dominated regime. *Chaos Applied to Fluid Mixing,* H. Aref and M. S. El Naschie, Eds., Pergamon Press, 347–366. [Also available in *Chaos, Soliton Fractals,* **4,** 1111–1116.]

——, 2000: Lattice models of advection–diffusion. *Chaos,* **10,** 61–74.

——, and H. Yang, 1993: Global chaotic mixing on isentropic surfaces. *J. Atmos. Sci.,* **50,** 2462–2480.

Shraiman, B. I., and E. D. Siggia, 1994: Lagrangian path integrals and fluctuations in random flows. *Phys. Rev.,* **49E,** 2912–2927.

Sinai, Y. G., and V. Yakhot, 1989: Limiting probability distributions

of a passive scalar in a random velocity field. *Phys. Rev. Lett.*, **63,** 1962–1964.

Sparling, L. C., 2000: Statistical perspectives on stratospheric transport. *Rev. Geophys.*, **38,** 417–436.

——, and J. T. Bacmeister, 2001: Scale dependence of tracer microstructure: PDF's, intermittency and the dissipation scale. *Geophys. Res. Lett.*, **28,** 2823–2826.

Strahan, S. E., and J. D. Mahlman, 1994: Evaluation of the SKYHI general circulation model using aircraft N_2O measurements, Part II: Tracer variability and diabatic meridional circulation. *J. Geophys. Res.*, **99,** 10 319–10 332.

Thoroddsen, S. T., and C. W. Van Atta, 1992: Exponential tails and skewness of density-gradient probability density functions in stably stratified turbulence. *J. Fluid Mech.*, **244,** 547–566.

Warhaft, Z., 2000: Passive scalars in turbulent flows. *Annu. Rev. Fluid Mech.*, **32,** 203–240.

Waugh, D. W., and Coauthors, 1997: Mixing of polar vortex air into middle latitudes as revealed by tracer–tracer scatter plots. *J. Geophys. Res.*, **102,** 13 119–13 134.

Yakhot, V., S. A. Orszag, S. Balachandar, E. Jackson, Z. She, and L. Sirovich, 1990: Phenomenological theory of probability distributions in turbulence. *J. Sci. Comput.*, **5,** 199–221.

Yuan, G., K. Nam, T. M. Antonsen Jr., E. Ott, and P. N. Guzdar, 2000: Power spectrum of passive scalars in two-dimensional chaotic flows. *Chaos*, **10,** 39–49.